Determination of spin-orbit coefficients in semiconductor quantum wells

S. Faniel,[1] T. Matsuura,[2] S. Mineshige,[1] Y. Sekine,[3] and T. Koga[1,2]

[1]*Division of Electronics for Informatics, Graduate School of Information Science and Technology, Hokkaido University, N-14, W-9, Kita-ku, Sapporo, Hokkaido 060-0814, Japan*

[2]*Creative Research Institution, Research Department, Hokkaido University, Hokkaido 001-0021, Japan*

[3]*NTT Basic Research Laboratories, NTT Corporation, Atsugi, Kanagawa 243-0198, Japan*

(Received 12 November 2010; published 7 March 2011)

We report the determination of the intrinsic spin-orbit interaction (SOI) parameters for $In_{0.53}Ga_{0.47}As/In_{0.52}Al_{0.48}As$ quantum wells (QWs) from the analysis of the weak antilocalization effect. We show that the Dresselhaus SOI is mostly negligible in this system and that the intrinsic parameter for the Rashba effect, $a_{SO} \equiv \alpha/\langle E_z \rangle$, is given to be $a_{SO}m^*/m_e = (1.46\text{–}1.51 \times 10^{-17} N_S\ [\mathrm{m}^{-2}])\ e\text{Å}^2$, where α is the Rashba SOI coefficient, $\langle E_z \rangle$ is the expected electric field within the QW, m^*/m_e is the electron effective mass ratio, and N_S is the sheet carrier density. These values for $a_{SO}m^*$ were also confirmed by the observation of beatings in the Shubnikov–de Haas oscillations in our most asymmetric QW sample.

DOI: 10.1103/PhysRevB.83.115309 PACS number(s): 73.63.Hs, 71.70.Ej, 73.23.Ad, 85.35.Ds

I. INTRODUCTION

As a result of the spin-orbit interaction (SOI), the conduction band of a semiconductor experiences spin splittings even at zero magnetic field, if the system lacks spatial inversion symmetry. In quantum well (QW) structures grown in the [001] direction out of zinc blende crystals,[1] the spin splittings induced by the bulk inversion asymmetry are the linear and cubic Dresselhaus spin splittings, whose effective Hamiltonians are $H_D^{(1)} = \beta_1 k\{\sigma_x \cos\theta - \sigma_y \sin\theta\}$ and $H_D^{(3)} = \beta_3 k^3\{\sigma_x \cos(3\theta) + \sigma_y \sin(3\theta)\}$, respectively,[2] where β_1 and β_3 are the Dresselhaus SOI coefficients, k the electron wave number, σ_x and σ_y the Pauli spin matrices, and θ the azimuthal angle for the wave vector $\mathbf{k} = (k_x, k_y) = (k\cos\theta, k\sin\theta)$. The Rashba spin splitting[3] arises from the structural inversion asymmetry in artificially grown heterostructures, whose effective Hamiltonian is $H_R = \alpha k\{\sigma_x \sin\theta - \sigma_y \cos\theta\}$, α being the Rashba SOI coefficient. β_1 and β_3 are both proportional to a single intrinsic parameter γ, referred to as the bulk Dresselhaus parameter.[4] The relations $\beta_1 = \gamma(\langle k_z^2 \rangle - \frac{k^2}{4})$ and $\beta_3 = \frac{\gamma}{4}$ are obtained from the effective mass approximation,[5] where $\langle k_z^2 \rangle$ denotes the expectation value of the operator $\hat{k}_z^2 \equiv -\frac{\partial^2}{\partial z^2}$ with the wave function along the confinement direction z. While it is envisioned that α should be proportional to $\langle E_z \rangle$, where $\langle E_z \rangle$ is the expectation value of the z component of the electric field in the pertinent QW excluding the interfacial contribution from the well-barrier boundary,[3,6] some debates also exist.[7] There are multiple mechanisms that would cause Rashba-type spin splittings besides $\langle E_z \rangle$, such as band discontinuities,[8,9] specific bonding arrangements at the heterointerfaces,[10] and the lattice-strain effect.[11] By and large, the relation $\alpha \propto \langle E_z \rangle$ is believed to hold in semiconductor QWs, where the value of the proportionality constant $a_{SO} \equiv \alpha/\langle E_z \rangle$ should be an intrinsic parameter of the material. The determination of the γ and a_{SO} values and the discovery of simple rules to predict the values of β_1, β_3, and α will not only play essential roles for the development of future spintronics[12–15] just in the same way the determination of the effective mass values did for the development of the conventional charge-based electronics,[16] but they will also provide useful checks for band-theory calculations. Thus, the establishment of experimental schemes to determine these SOI coefficients are of paramount importance.

In this paper, we report on the experimental determination of the intrinsic parameter a_{SO} in $In_{0.53}Ga_{0.47}As$ /$In_{0.52}Al_{0.48}As$ QWs[17] using low temperature magnetoconductance measurements. Thus far, the SOI-related spin splittings have been studied through the beatings in the Shubnikov–de Haas (SdH) oscillations,[9,18,19] analysis of the weak antilocalization (WAL) dips in magnetoconductance measurements,[17,20,21] the spin-Galvanic effect,[13] spin-flip Raman scattering,[22] electron spin resonance,[23] and time-resolved Faraday rotation.[11,24] In these measurements, even if the observed spin splittings were considered to be the Rashba type, they were rarely correlated with $\langle E_z \rangle$ to deduce the values of a_{SO}. Besides that $\langle E_z \rangle$ is not a directly measurable quantity, the difficulties also come from the complicated process of disentangling the values of α, β_1, and β_3 from the measured spin splittings.

In the following section, using the symmetrically doped sample KH1-3 (see Appendix A), we will see that the WAL effect is clearly minimized at some carrier density N_S^*, where $\langle E_z \rangle = 0$ is realized (Sec. II A). We then obtain the values αm^* from fits to the low-field magnetoconductance data using the Golub model,[25] where m^* is the electron effective mass, neglecting $H_D^{(1)}$ and $H_D^{(3)}$ over H_R (Sec. II B). The parameter values prerequisite in this analysis are only the electron mean free path and the electron density, both of which are obtainable from the Hall and/or SdH measurements directly, making the purely experimental determination of αm^* values possible.

II. EXPERIMENT

The heterostructures investigated are lattice-matched, 10 nm–thick $In_{0.53}Ga_{0.47}As/In_{0.52}Al_{0.48}As$ QWs grown by metal organic chemical vapor deposition on (001) InP substrates.[26] We studied 10 different QWs with various doping profiles (see Appendix A). $In_{0.53}Ga_{0.47}As/In_{0.52}Al_{0.48}As$ is a technologically important material system for future spintronics because of its strain-free nature, relatively large spin splitting energies, and stable gate-controllability, where the last factor was made possible owing to recent developments in high-κ gate insulators.[27]

Standard Hall bar samples were fabricated using either a 20 nm–thick HfO_2 layer (atomic layer deposition) or a 100 nm–thick SiO_2 layer (evaporation) as gate dielectric. The magnetoconductance measurements were performed at the base temperatures of dilution ($T \sim 30$ mK) or ^{3}He ($T \sim 300$ mK) refrigerators with the magnetic field B applied perpendicular to the plane of the QW. The electric characterizations were done using a standard lock-in technique with an electric current of ~100 nA and frequencies between 11 and 183 Hz.

A. Determination of the bulk Dresselhaus parameter γ

Shown in Fig. 1 are the measured magnetoconductance traces $\sigma(B)$ for a symmetrically doped sample (KH1-3) at several values of gate-controlled N_S. The negative magnetoconductances, a characteristic signature of the WAL effect, are clearly seen in all traces in the vanishing B. A measure of the SOI strength is provided by the characteristic field for the SOI, B_{SO}, which is given as $B_{SO} \equiv \alpha^2 m^{*2}/e\hbar^3$ for the case of the Rashba spin splitting.[28] Empirically, the values of B_{SO} are approximated by the magnetic field where $\sigma(B)$ is minimized, denoted as B_{min} (see vertical marks in Fig. 1). Equating B_{min} to B_{SO}, we obtain a phenomenological SOI coefficient $\tilde{\alpha}m^* = \sqrt{e\hbar^3 B_{min}}$. In Fig. 2, we find that such $\tilde{\alpha}m^*$ has a V-shaped dip as a function of N_S ($N_S^* = 1.06 \times 10^{16}$ m^{-2}, where $\tilde{\alpha}m^*$ is minimized). In the presence of both the Dresselhaus and Rashba SOIs, the WAL effect is expected to be weakened if $\alpha = \pm\beta_1$,[14,15,29] suggesting a double dip feature in the $\tilde{\alpha}m^*$ vs N_S curve. However, in our measurements, we observed the weakening of $\tilde{\alpha}m^*$ at only one N_S.

This single minimum behavior in the $\tilde{\alpha}m^*$ vs N_S relation suggests either (1) β_1 is so small that the $\alpha = \pm\beta_1$ conditions are merged together into a single dip, or (2) β_1 is so large that the second minimum is not visible in the investigated N_S range. The latter interpretation is ruled out since large β_1 values also imply a strong contribution from $H_D^{(3)}$ which is inconsistent with the minimum value of $\tilde{\alpha}m^*$ observed at N_S^* ($\tilde{\alpha}m^*/m_e = 7.5 \times 10^{-15}$ eV m).[30] The minimum in the $\tilde{\alpha}m^*$ vs N_S curve then corresponds to the condition where the QW is made symmetric; i.e., $\langle E_z \rangle = 0$ at N_S^*.

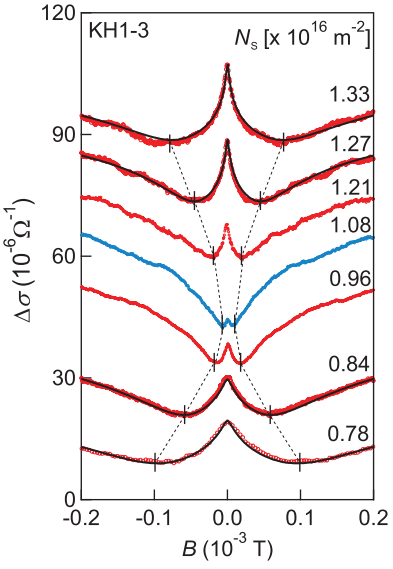

FIG. 1. (Color online) Magnetoconductances of a gated-$In_{0.53}Ga_{0.47}As$ QW (KH1-3) for various values of N_S. Each trace has been shifted vertically. The solid curves show the fits to the data by the Golub model.[25] The position of B_{min} is indicated by vertical marks in each trace. The dashed lines are guides to the eye.

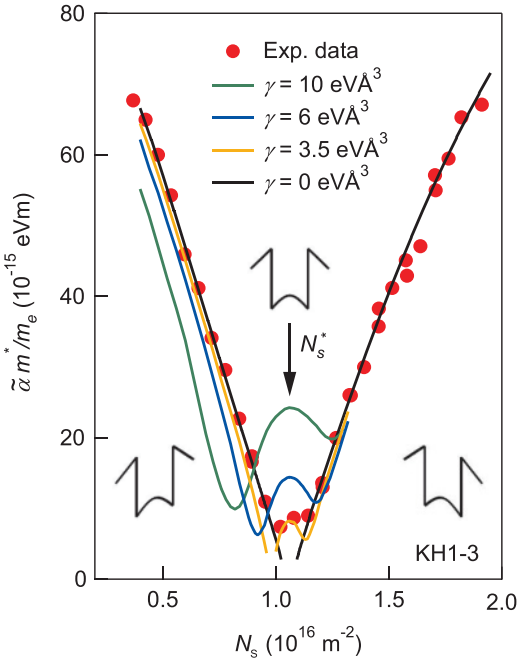

FIG. 2. (Color online) The phenomenological SOI coefficient $\tilde{\alpha}m^*$ extracted from the B_{min} values in Fig 1. The solid lines are calculations obtained using the Knap ($\gamma = 3.5,6$, and 10 eV Å^3) and Golub ($\gamma = 0$ eV Å^3) models. The vertical arrow indicates the density N_S^*, where the QW is made symmetric; i.e., $\langle E_z \rangle = 0$.

We estimated the value of γ as follows. Shown together in Fig. 2 are the simulated values of $\tilde{\alpha}m^*$, extracted from the theoretically modeled magnetoconductance curves including the Rashba and Dresselhaus spin splittings and assuming $\gamma = 0,3.5,6$, and 10 eV Å^3, using the theoretical models developed by Golub[25] ($\gamma = 0$ eV Å^3) and Knap *et al.*[5] ($\gamma = 3.5,6$, and 10 eV Å^3). In these calculations, we used Eq. (4) for the Rashba spin splittings with $N_S^* = 1.06 \times 10^{16}$ m^{-2}, which will be justified later, and assumed $\tau_3 = \tau_{tr}$ when using the Knap model. Here τ_{tr} is the transport scattering time and τ_3 is a higher order scattering time defined as[5]

$$\frac{1}{\tau_3} = \int_0^\pi W(\theta)[1 - \cos(3\theta)]\, d\theta, \qquad (1)$$

where $W(\theta)$ is the probability of scattering by an angle θ. The value of this parameter depends on details of the scattering mechanism—for example, $\tau_3^{-1}/\tau_{tr}^{-1} = 1$ for isotropic scattering and $\tau_3^{-1}/\tau_{tr}^{-1} = 9$ for small-angle scattering.[5] In Fig. 2, the condition $B_{SO} \ll B_{tr}$, required in the Knap model, is satisfied at N_S smaller than 1.3×10^{16} m^{-2}, where B_{tr} is a characteristic magnetic field relevant to τ_{tr}, so that the theoretical $\tilde{\alpha}m^*$ data for $\gamma = 3.5,6$, and 10 eV Å^3 are limited to this range.[31] We found that the simulated $\tilde{\alpha}m^*$ vs N_S curves substantially deviate from the experimental one if $\gamma >$

3.5 eV Å^3. Thus, we regard the value 3.5 eV Å^3 as a reasonable upper limit for the experimental γ. For $\gamma \lesssim 3.5$ eV Å^3, the double dip of the $\tilde{\alpha}m^*$ vs N_S curves is restricted to a narrow N_S range around N_S^*, where the calculated values of $\tilde{\alpha}m^*$ underestimate the experimental ones[32] (see Appendix B). This discrepancy suggests the presence of additional spin relaxation mechanisms[33] not included in the theoretical model, or spatial variations of α in the sample, reflecting that of the doping density and/or the QW thickness $d_{\rm QW}$.

We note that the above estimated value of γ is smaller than the predicted values in $\mathbf{k}\cdot\mathbf{p}$ theory ($\gamma \sim 27$ eV Å^3).[5,34] A similar observation is found in a recent experiment by Zhou *et al.*[35] The γ values for GaAs QWs ($\gamma \sim 5$ eV Å^3) are also known to be reduced from the $\mathbf{k}\cdot\mathbf{p}$ value for bulk GaAs ($\gamma \sim 27$ eV Å^3).[15,36] After all, we conclude that $\gamma \lesssim 3.5$ eV Å^3 in (001)$In_{0.53}Ga_{0.47}As$(10 nm)/$In_{0.52}Al_{0.48}As$ QWs. Thus, $H_D^{(1)}$ and $H_D^{(3)}$ may be neglected relative to H_R in most cases except at $N_S = N_S^*$ even with sample KH1-3.

B. Determination of the intrinsic parameter for the Rashba effect

Having shown that $H_D^{(1)}$ and $H_D^{(3)}$ may be neglected relative to H_R, we fitted the experimental $\sigma(B)$ data with the WAL theory developed by Golub recently,[25] assuming only Rashba-type spin splitting, for accurate deduction of the αm^* values. In contrast to the previous theoretical models,[5,28] valid only for $B_{\rm SO} \ll B_{\rm tr}$ and $B \ll B_{\rm tr}$, the new theory is valid for all magnetic field ranges and Rashba coefficient α values.[21] The excellent quality for the fittings of the WAL data by this model is found in Fig. 1. We also note that it is the value of the product αm^*, not the value of α, that is deducible directly from experiment. Thus, the value of the product $a_{\rm SO}m^*$ is obtained purely experimentally without assuming any values of other parameters, as below.

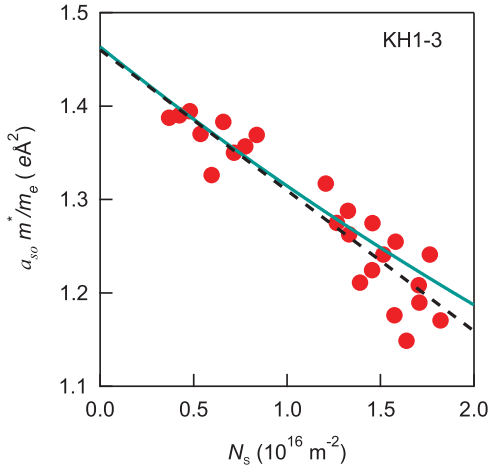

FIG. 3. (Color online) The extracted values of $a_{\rm SO}m^*$ as a function of N_S for KH1-3. The dashed line is a linear fit to the data. The solid curve shows the values of $r_{41}^{6c6c}m^*$ calculated using Eqs. (2) and (4), replacing E_g with $(E_g + E_F)$ and multiplied by 1.68 (see text).

Plotted in Fig. 3 are the values of the intrinsic parameter $a_{\rm SO}m^* \equiv \alpha m^*/\langle E_z\rangle$ as a function of N_S, where $\langle E_z\rangle$ is given as $\frac{|e|}{2\epsilon_s\epsilon_0}(N_S^* - N_S)$ directly from the Poisson equation through the integration by parts[34] assuming that electrons are entirely confined within the QW, and the dielectric constant used is $\epsilon_s = 13.1$. We note that the positive and negative values were assigned for α at N_S smaller and larger than N_S^*, respectively, reflecting the sign of $\langle E_z\rangle$. It turned out that the obtained $a_{\rm SO}m^*/m_e$ values decrease with increasing N_S. A linear regression to the experimental data, assuming the formula $a_{\rm SO}m^*/m_e = a - bN_S$, gave the parameter values $a = 1.46\ e$Å^2 and $b = 1.51 \times 10^{-17}\ e$Å^2 m^2.

III. DISCUSSION

A. Comparison with k · p theory

We now compare the values of $a_{\rm SO}m^*$ obtained in our analysis with predictions from $\mathbf{k}\cdot\mathbf{p}$ theory. In third-order perturbation theory using the extended Kane model, the leading terms of the bulk effective mass m^* and r_{41}^{6c6c}, the bulk counterpart of $a_{\rm SO}$, are respectively given as

$$\frac{m_e}{m^*} = 1 + \frac{2m_e}{\hbar^2}\frac{P^2}{3}\left(\frac{2}{E_g} + \frac{1}{E_g + \Delta_{\rm SO}}\right) \tag{2}$$

and

$$r_{41}^{6c6c} = \frac{eP^2}{3}\frac{2\Delta_{\rm SO}(E_g + \Delta_{\rm SO}/2)}{E_g^2(E_g + \Delta_{\rm SO})^2}, \tag{3}$$

where E_g is the band gap energy, $\Delta_{\rm SO}$ is the spin-orbit split-off energy, and P is the momentum matrix element.[34] Putting the band parameter values for $In_{0.53}Ga_{0.47}As$,[17,34] we obtain the value $r_{41}^{6c6c}m^*/m_e = 0.87\ e$Å^2, which is about 60% of the experimental value of a. For the observed N_S dependence of $a_{\rm SO}m^*$, we note that increasing the Fermi energy E_F has a similar effect as increasing the effective band gap energy.[34,37] Replacing E_g in Eqs. (2) and (3) with $(E_g + E_F)$, the N_S dependence of $r_{41}^{6c6c}m^*/m_e$ was naively simulated. We then find that the theoretical value of b was also 60% of the corresponding experimental value (see Fig. 3). The contribution from the valence band discontinuities at the well-barrier interfaces to the SOI can be incorporated into the model by adding the prefactor $(\Delta E_c + \Delta E_v)/\Delta E_c \approx 1.4$ to Eq. (3), where ΔE_c and ΔE_v are the conduction and valence band offsets.[34] When including the band discontinuity effect in this way, the theoretical $r_{41}^{6c6c}m^*$ is 84% of the experimental $a_{\rm SO}m^*$. The values of $a_{\rm SO}m^*$ extracted from our experimental data are thus found to be in reasonable agreement with $\mathbf{k}\cdot\mathbf{p}$ theory.

B. Applicability of the obtained $a_{\rm SO}m^*$ values to the other asymmetric quantum wells

The applicability of the obtained $a_{\rm SO}m^*$ values as a function of N_S was checked with the αm^* vs N_S data obtained for the other 10 nm–thick $In_{0.53}Ga_{0.47}As/In_{0.52}Al_{0.48}As$ QWs that have different back doping densities N_1^+ than KH1-3. All these samples showed strong WAL effects in the low temperature magnetoconductance data $\sigma(B)$, where we deduced the α values as a function of N_S for each sample from the fittings

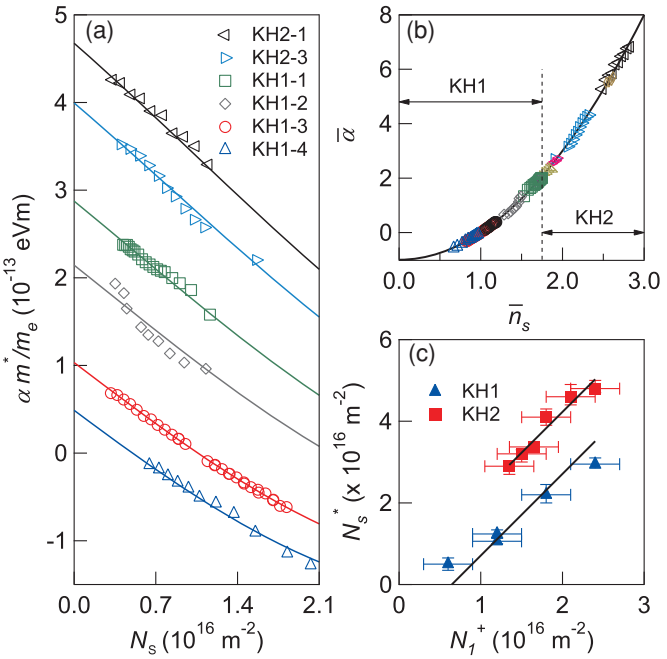

FIG. 4. (Color online) (a) The Rashba parameter αm^* as a function of N_S. The symbols denote the experimental values extracted from the WAL analysis. The solid curves are the fits using Eq. (4). (b) The scaled Rashba parameter values $\bar{\alpha}$ as a function of the scaled electronic density $\bar{n}_S$ for all the investigated QWs including those not shown in (a). The relation $\bar{\alpha} = \bar{n}_S^2 - 1$ is shown by the solid curve. (c) Virtual electronic densities N_S^* which correspond to the $\langle E_z \rangle = 0$ condition as a function of the doping density N_1^+ in the substrate side of the QWs. The solid lines show the expected relation between N_S^* and N_1^+ (line with slope 2). The error bars for N_1^+ and N_S^* represent typical uncertainties by growth and fits to the αm^* vs N_S curves using Eq. (4), respectively.

with Golub theory as in Fig. 4(a). The experimental αm^* vs N_S data were then fitted with the equation

$$\alpha m^*/m_e = \frac{|e|}{2\epsilon_s \epsilon_0}(a - bN_S)(N_S^* - N_S). \qquad (4)$$

Here, N_S^* was used as a fitting parameter, which only virtually corresponds to the $\langle E_z \rangle = 0$ condition in these QWs. As shown in Fig. 4(a), the experimental αm^* vs N_S curves are well fitted with Eq. (4) in all samples, if the value of N_S^* is properly chosen. The generality and applicability of Eq. (4) is summarized in the scaled plot in Fig. 4(b), where the scaled variable $\bar{\alpha} \equiv \alpha m^* \frac{8b\epsilon_s\epsilon_0}{(a-bN_S^*)^2|e|}$ is plotted as a function of $\bar{n}_S \equiv -\frac{2bN_S - a - bN_S^*}{a - bN_S^*}$ for all the epiwafers used in the experiment. We find that all the experimental data collapse on a single universal curve $\bar{\alpha} = \bar{n}_S^2 - 1$. The validity of our analysis using Eq. (4) is also backed up by the correlation observed between the values of N_S^* and N_1^+. We note that the change in N_1^+, denoted as ΔN_1^+, should accompany the change in N_S^* by $2\Delta N_1^+$, if no other background impurities are present below QW and the boundary condition (or the position of the Fermi energy pinning) is kept constant at the buffer layer/substrate interface among the samples, which is roughly the case for a series of samples that were grown under the same growth calibration. This relation is checked for two series of samples investigated [Fig. 4(c)], named KH1-ξ (ξ = 1–4) and KH2-η (η = 1–6). As shown in Fig. 4(c), good correlations were found between N_S^* and N_1^+ with slope 2 for both KH1 and KH2 samples, as expected.

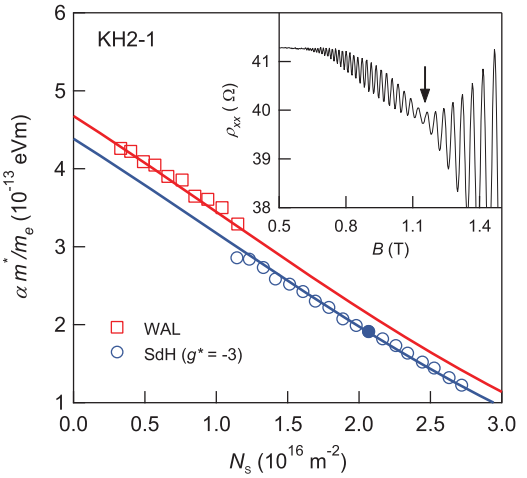

FIG. 5. (Color online) The Rashba parameter αm^* as a function of N_S extracted for KH2-1 from the WAL (open squares) and SdH (open circles) analyses. The solid curves are the fits using Eq. (4). Inset: Beating in the SdH oscillation observed at $N_S = 2.07 \times 10^{16}$ m^{-2}. The arrow indicates the position of the beating node used for the extraction of the αm^* value (filled circle in the main figure). Measurements were performed at $T = 30$ mK (base temperature).

C. Confirmation by the SdH beating

We finally report our observation of the SdH beating with one of our samples that has the largest Rashba spin splitting (KH2-1). An example of such SdH beating patterns is shown in the inset of Fig. 5. In QW samples with well-defined Landau levels, beating nodes appear in the SdH oscillation at magnetic fields where the spin-splitting energy δ ($\delta \to 2\alpha k_F$ for $B \to 0$) is an odd multiple of $\hbar\omega_c/2$, where $\omega_c = |e|B/m^*$.[19] Theoretically, the value of δ is obtained by direct diagonalization of the Hamiltonian matrix using the Landau quantization basis in the presence of the Rashba and Zeeman terms:[19]

$$\delta = \{[\hbar\omega_c(1 - g^* m^*/2m_e)]^2 + (2\alpha k_F)^2\}^{\frac{1}{2}} - \hbar\omega_c\,, \qquad (5)$$

where g^* is the effective Landé g factor and k_F is the Fermi wave number. For sample KH2-1, we observed only one node corresponding to $\delta = \hbar\omega_c/2$. Assuming $m^*/m_e = 0.047$,[17] and $g^* = -3$,[38] the extracted values of αm^* were plotted as a function of N_S in Fig. 5 together with those obtained from the WAL analysis for the same epiwafer (KH2-1). A reasonable agreement is found between the αm^* values from the SdH beating and those from the WAL analysis, similar to previous studies in strained InGaAs QWs.[21] A good fit was also obtained for the αm^* vs N_S data from the SdH beating using Eq. (4), where the value of N_S^* turned out to be about 7% smaller than that from the WAL analysis. This discrepancy may be due to the fluctuations in the back and/or front doping

densities, namely N_1^+ and/or N_2^+, either spatially or by thermal cycling.

IV. CONCLUSION

As a conclusion, we have deduced the values of the intrinsic parameter $a_{SO}m^*/m_e$, which relates the Rashba coefficient α to the averaged electric field within the quantum well $\langle E_z \rangle$, to be $(1.46–1.51\times10^{-17}\ N_S\ [\mathrm{m}^{-2}])\ e\text{Å}^2$, irrespective of the QW's doping profile, for (001) oriented, 10 nm–thick gated-$In_{0.53}Ga_{0.47}As/In_{0.52}Al_{0.48}As$ QWs. We have also estimated the value of the bulk Dresselhaus parameter γ to be $\lesssim$3.5 eV Å^3, implying that the linear and cubic Dresselhaus SOIs are negligible relative to the Rashba SOI in our QWs unless the condition $\langle E_z \rangle \approx 0$ is realized. The quantitative determination of these fundamental parameters is essential for designing semiconductor systems with tailored spin-orbit properties, and provides a useful reference to test band-theory calculations.

ACKNOWLEDGMENTS

The authors are indebted to Dr. H. Yokoyama and Dr. H. Sugiyama for sample growth, to Professors R. Winkler, L. E. Golub, G. Yu, and J. Nitta for fruitful discussions, and to Dr. K. Sueoka and Dr. T. Akazaki for support. This work was partially supported by KAKENHI, Grant-in-Aid for Young Scientists (A), No. 19684009. S. Faniel thanks the JSPS for financial support.

APPENDIX A

The heterostructures investigated here are lattice-matched, 10 nm–thick, $In_{0.53}Ga_{0.47}As/In_{0.52}Al_{0.48}$ QWs grown by metal organic chemical vapor deposition (MOCVD) on (001) InP substrates. The growth sequence of the QWs is illustrated in Fig. 6 and all specific growth parameters are summarized Table I.

APPENDIX B

In Fig. 2, the condition $\tau_3^{-1}/\tau_{tr}^{-1} = 1$ may overcount the effect of $H_D^{(3)}$ in the simulated magnetoconductance curves

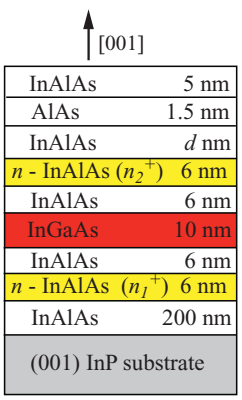

FIG. 6. (Color online) Schematic illustration of the growth sequence for the $In_{0.53}Ga_{0.47}As/In_{0.52}Al_{0.48}As$ QWs.

TABLE I. Growth parameters for the investigated quantum wells: n_1^+ and n_2^+ are the back and front doping densities by Si dopant, respectively, and d is the thickness of the $In_{0.52}Al_{0.48}As$ Schottky layer. The parameters n_1^+ and n_2^+ are given in (10^{18} cm^{-3}), and d in nm. Note that $N_{1,2}^+ = n_{1,2}^+ \times 6$ nm.

Wafer	n_1^+	n_2^+	d
KH1-1	4	0	20
KH1-2	3	1	20
KH1-3	2	2	20
KH1-4	1	3	20
KH2-1	4	0	20
KH2-2	3.5	0.5	20
KH2-3	3	1	25
KH2-4	2.75	1.25	25
KH2-5	2.5	1.5	25
KH2-6	2.25	1.75	25

through the parameter value of $\Omega_3^2\tau_3$ ($\Omega_3 = \beta_3 k^3$) in the Knap model,[5] because the comparison of the quantum scattering time τ_q and the transport scattering time τ_{tr} suggests that

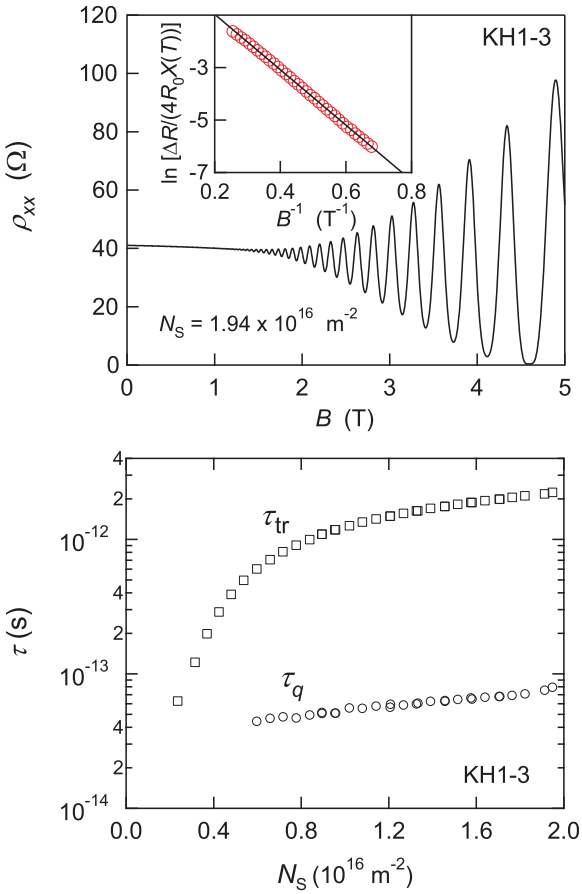

FIG. 7. (Color online) Top panel: Magnetoconductance of KH1-3 at $N_S = 1.94 \times 10^{16}$ m^{-2}, showing the SdH oscillation. Inset: Dingle plot of the SdH data. The red circles are the experimental data and the plain line is a linear fit to extract the value of τ_q. Bottom panel: Transport scattering time τ_{tr} and the quantum scattering time τ_q as a function of N_S for sample KH1-3. Measurements were performed at $T = 30$ mK (base temperature).

forward scatterings dominate in our samples ($\tau_3^{-1}/\tau_{\rm tr}^{-1} > 1$). The transport scattering time $\tau_{\rm tr}$ is mostly sensitive to large-angle scattering and rather insensitive to small-angle scattering, while the quantum scattering time τ_q depends on all scattering events. The quantum scattering time τ_q is defined as[39]

$$\frac{1}{\tau_q} = \int_0^{\pi} W(\theta)\, d\theta, \tag{B1}$$

and also provides a measure of the broadening of the Landau levels. This parameter can be extracted from Dingle plots of the Shubnikov–de Haas data as in Ref. 39. The amplitude of the SdH oscillation ΔR is given by

$$\Delta R = 4R_0 X(T) \exp\left(\frac{-\pi}{\omega_c \tau_q}\right), \tag{B2}$$

where

$$X(T) = \frac{2\pi^2 k_B T/\hbar\omega_c}{\sinh\left(2\pi^2 k_B T/\hbar\omega_c\right)}. \tag{B3}$$

Here, R_0 is the resistivity at $B = 0$, k_B is the Boltzmann constant, T is the temperature and ω_c is the cyclotron frequency. An example Dingle plot is shown in Fig. 7 for KH1-3 at $N_S = 1.94 \times 10^{16}$ m^{-2}. The transport scattering time $\tau_{\rm tr}$ and the quantum scattering time τ_q are displayed in Fig. 7 as a function of N_S, for the KH1-3 sample. The quantum scattering time τ_q is found to be typically 1/20 of $\tau_{\rm tr}$, indicating that forward scatterings dominate in our quantum wells. The assumption $\tau_3^{-1}/\tau_{\rm tr}^{-1} = 9$ in the Knap calculation, consistent with forward scattering, reduces the $H_D^{(3)}$ contribution to the WAL effect further, leading to a further underestimation, in turn, of the experimental $\tilde{\alpha} m^*$ in the vicinity of N_S^*.[32]

[1] Our crystallographic indices are defined placing the group III and V atoms in the [000] and $\frac{a}{4}$[111] positions in the unit cell, respectively, where a is the lattice constant.

[2] $\hat{x} \parallel [100]$, $\hat{y} \parallel [010]$, and $\hat{z} \parallel [001]$. $\hat{z}$ is normal to the sample surface.

[3] E. I. Rashba, Fiz. Tverd. Tela **2**, 1224 (1960) [Sov. Phys. Solid State **2**, 1109 (1960)]; Y. A. Bychkov and E. I. Rashba, J. Phys. C **17**, 6039 (1984).

[4] G. Dresselhaus, Phys. Rev. **2**, 580 (1955).

[5] W. Knap *et al.*, Phys. Rev. B **53**, 3912 (1996).

[6] F. J. Ohkawa and Y. Uemura, J. Phys. Soc. Jpn. **37**, 1325 (1974).

[7] A. Därr, J. P. Kotthaus, and T. Ando, in *Proceedings of the 13th International Conference on the Physics of Semiconductors*, edited by F. G. Fumi (North-Holland, Amsterdam, 1976), p. 774; R. Lassnig, Phys. Rev. B **31**, 8076 (1985); S. Brosig, K. Ensslin, R. J. Warburton, C. Nguyen, B. Brar, M. Thomas, and H. Kroemer, *ibid.* **60**, R13989 (1999); A. C. H. Rowe, J. Nehls, R. A. Stradling, and R. S. Ferguson, *ibid.* **63**, 201307 (2001).

[8] P. Pfeffer and W. Zawadzki, Phys. Rev. B **52**, R14332 (1995).

[9] G. Engels, J. Lange, T. Schäpers, and H. Lüth, Phys. Rev. B **55**, R1958 (1997).

[10] B. Jenichen, S. A. Stepanov, B. Brar, and H. Kroemer, J. Appl. Phys. **79**, 120 (1996).

[11] Y. K. Kato, R. C. Myers, A. C. Gossard, and D. D. Awschalom, Science **306**, 1910 (2004).

[12] S. Datta and B. Das, Appl. Phys. Lett. **56**, 665 (1990); H. C. Koo, J. H. Kwon, J. Eom, J. Chang, S. H. Han, and M. Johnson, Science **325**, 1515 (2009); K. C. Nowack, F. H. L. Koppens, Yu. V. Nazarov, and L. M. K. Vandersypen, *ibid.* **318**, 1430 (2007); T. Koga, J. Nitta, H. Takayanagi, and S. Datta, Phys. Rev. Lett. **88**, 126601 (2002); S. M. Frolov, S. Lüscher, W. Yu, Y. Ren, J. A. Folk, and W. Wegscheider, Nature (London) **458**, 868 (2009); Y. Kato, R. C. Myers, D. C. Driscoll, A. C. Gossard, J. Levy, and D. D. Awschalom, Science **299**, 1201 (2003).

[13] S. D. Ganichev, E. L. Ivchenko, V. V. Bel'kov, S. A. Tarasenko, M. Sollinger, D. Weiss, W. Wegscheider, and W. Prettl, Nature (London) **417**, 153 (2002).

[14] B. A. Bernevig, T. L. Hughes, and S.-C. Zhang, Science **314**, 1757 (2006).

[15] J. D. Koralek, C. P. Weber, J. Orenstein, B. A. Bernevig, S.-C. Zhang, S. Mack, and D. D. Awschalom, Nature (London) **458**, 610 (2009).

[16] L. Esaki, Phys. Scr. T **42**, 102 (1992).

[17] T. Koga, J. Nitta, T. Akazaki, and H. Takayanagi, Phys. Rev. Lett. **89**, 046801 (2002).

[18] B. Das, D. C. Miller, S. Datta, R. Reifenberger, W. P. Hong, P. K. Bhattacharya, J. Singh, and M. Jaffe, Phys. Rev. B **39**, 1411 (1989); J. Luo, H. Munekata, F. F. Fang, and P. J. Stiles, *ibid.* **41**, 7685 (1990); J. Nitta, T. Akazaki, H. Takayanagi, and T. Enoki, Phys. Rev. Lett. **78**, 1335 (1997).

[19] B. Das, S. Datta, and R. Reifenberger, Phys. Rev. B **41**, 8278 (1990).

[20] P. D. Dresselhaus, C. M. A. Papavassiliou, R. G. Wheeler, and R. N. Sacks, Phys. Rev. Lett. **68**, 106 (1992); G. L. Chen, J. Han, T. T. Huang, S. Datta, and D. B. Janes, Phys. Rev. B **47**, 4084 (1993).

[21] V. A. Guzenko, T. Schäpers, and H. Hardtdegen, Phys. Rev. B **76**, 165301 (2007).

[22] B. Jusserand, D. Richards, H. Peric, and B. Etienne, Phys. Rev. Lett. **69**, 848 (1992); D. Richards and B. Jusserand, Phys. Rev. B **59**, 2506(R) (1999).

[23] M. Schulte, J. G. S. Lok, G. Denninger, and W. Dietsche, Phys. Rev. Lett. **94**, 137601 (2005).

[24] L. Meier, G. Salis, I. Shorubalko, E. Gini, S. Schön, and K. Ensslin, Nature Phys. **3**, 650 (2007).

[25] L. E. Golub, Phys. Rev. B **71**, 235310 (2005).

[26] H. Sugiyama, K. Watanabe, H. Yokoyama, and T. Kobayashi, J. Appl. Phys. **93**, 4260 (2003); H. Sugiyama, H. Yokoyama, and K. Wada, Jpn. J. Appl. Phys. **38**, 1158 (1999).

[27] I. J. Gelfand, S. Amasha, D. M. Zumbühl, M. A. Kastner, C. Kadow, and A. C. Gossard, Appl. Phys. Lett. **88**, 252105 (2006); J. Sun, M. Larsson, I. Maximov, and H. Q. Xu, *ibid.* **96**, 162107 (2010).

[28] S. V. Iordanskii, Yu. B. Lyanda-Geller, and G. E. Pikus, JETP Lett. **60**, 206 (1994).

[29] J. Schliemann and D. Loss, Phys. Rev. B **68**, 165311 (2003).

[30]We obtain $\gamma = 6$ eV Å^3 if we attribute this solely to $H_D^{(3)}$, assuming $\tau_3 = \tau_{\rm tr}$.

[31]The exact criterion used here is $B_{\rm SO} < \frac{1}{4} B_{\rm tr}$.

[32]S. Faniel, T. Matsuura, S. Mineshige, Y. Sekine, and T. Koga, in *Proceedings of the 30th International Conference on the Physics of Semiconductors* (to be published).

[33]G. E. Pikus and A. N. Titkov, in *Optical Orientation* (Elsevier, Amsterdam, 1984).

[34]R. Winkler, in *Spin-Orbit Coupling Effects in Two-Dimensional Electron and Hole Systems* (Springer-Verlag, Berlin, Heidelberg, 2003).

[35]Y. M. Zhou, G. Yu, L. M. Wei, K. H. Gao, W. Z. Zhou, T. Lin, L. Y. Shang, S. L. Guo, J. H. Chu, N. Dai, and D. G. Austing, J. Appl. Phys. **107**, 053708 (2010).

[36]J. J. Krich and B. I. Halperin, Phys. Rev. Lett. **98**, 226802 (2007); see also EPAPS Document No. E-PRLTAO-98-029722.

[37]T. Schäpers, G. Engels, J. Lange, T. Klocke, M. Hollfelder, and H. Lüth, J. Appl. Phys. **83**, 4324 (1998); W. Yang and Kai Chang, Phys. Rev. B **74**, 193314 (2006).

[38]F. E. Meijer, A. F. Morpurgo, T. M. Klapwijk, T. Koga, and J. Nitta, Phys. Rev. B **70**, 201307(R) (2004).

[39]P. T. Coleridge, Phys. Rev. B **44**, 3793 (1991).